

Phonon mediated spin relaxation in a moving quantum dot: Doppler shift, Cherenkov radiation, and spin relaxation boom

Xinyu Zhao^{1,*}, Peihao Huang^{1,2,†} and Xuedong Hu^{1,‡}

¹*Department of Physics, University at Buffalo, SUNY, Buffalo, New York 14260, USA and*

²*Department of Physics, California State University Northridge, Northridge, California 91330, USA*

We study relaxation of a moving spin qubit caused by phonon noise. As we vary the speed of the qubit, we observe several interesting features in spin relaxation and the associated phonon emission, induced by Doppler effect. In particular, in the supersonic regime, the phonons emitted by the relaxing qubit is concentrated along certain directions, similar to the shock waves produced in classical Cherenkov effect. As the speed of the moving qubit increases from the subsonic regime to the supersonic regime, the qubit experiences a peak in the spin relaxation rate near the speed of sound, which we term a spin relaxation boom in analogy to the classical sonic boom. We also find that the moving spin qubit may have a lower relaxation rate than a static qubit, which hints at the possibility of coherence-preserving transportation for a spin qubit. While the physics we have studied here has strong classical analogies, we do find that quantum confinement for the spin qubit plays an important role in all the phenomena we observe. Specifically, it produces a correction on the Cherenkov angle, and removes the divergence in relaxation rate at the sonic barrier. It is our hope that our results would encourage further research into approaches for transferring and preserving quantum information in spin qubit architectures.

PACS numbers: 72.25.Rb, 03.67.Hk, 03.67.Lx

I. INTRODUCTION

Electron spin qubit is a promising candidate for realizing quantum computing because of its long coherence time [1–4]. It has attracted extensive research interests over the past decade, with studies mostly focusing on the fabrication and manipulation of spin qubits confined in a fixed quantum dot or dopant ion [5–7].

In a large-scale quantum information processor, it is inevitable that quantum information is transferred over finite distances frequently. One straightforward way to achieve such communication is to move the qubits themselves directly. There are several proposed schemes on how to move spin qubits efficiently [8–16], where the motion of the confined electron can be induced by either varying gate voltages or a surface acoustic wave (SAW). However, introducing this orbital (albeit controlled) dynamics could weaken the orbital quantization that gives rise to the long spin coherence times. For instance, in Ref. [17] we have shown how electrostatic disorder in the substrate may cause relaxation of a moving spin qubit through spin-orbit interaction. Nevertheless, more studies are still needed to clarify decoherence of a moving spin qubit.

Doppler effect is a commonly observed phenomenon when an object is moving, where an observer hears different pitches from the horn of an approaching and a departing vehicle. When the velocity of the object is larger than the speed of the waves produced by the motion, a directional shock wave (Cherenkov effect) can be observed,

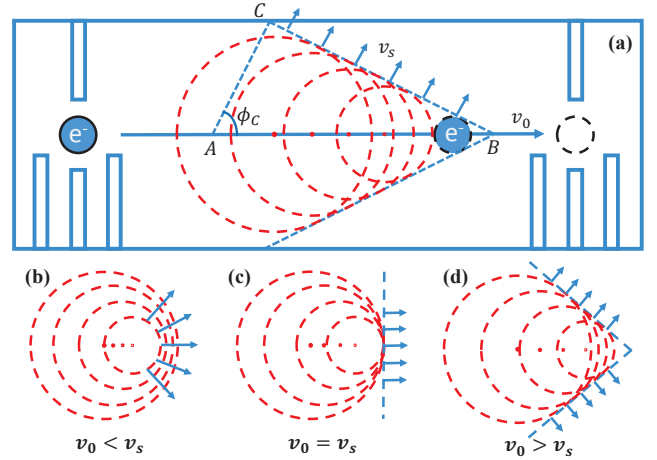


Figure 1. (color online) A schematic diagram of a moving spin qubit interacting with phonon reservoir and the resultant Doppler effect in the three cases.

from the wake of a speeding boat, to the sonic boom from a supersonic airplane, to Cherenkov radiation from a fast-moving charge in a material with high refraction index [18–21]. Classically (as depicted in Fig. 1), a superposition of the spherical waves emitted by a moving object at different moments form a straight-line wavefront BC , and the wavefront propagates in the AC direction, at the Cherenkov angle from the motion direction:

$$\cos \phi_C = \frac{AC}{AB} = \frac{v_s}{v_0}. \quad (1)$$

Since Cherenkov radiation is highly directional, it is often used to detect properties of moving charged particles.

Here we study how motion of a spin qubit could modify

* xzhao34@buffalo.edu

† peihao.huang@csun.edu

‡ xhu@buffalo.edu

its relaxation due to spin-orbit interaction and electron-phonon interaction [22–25]. In particular, we identify different regimes of quantum dot moving velocity where we can find analogues of Doppler effect, Cherenkov radiation, and sonic boom in the spin relaxation and the associated phonon emission. More specifically, when the quantum dot (QD) moves with a speed lower than the speed of sound, the energy of an emitted phonon is dependent on the direction of emission, similar to the Doppler effect. When the QD moves faster than the speed of sound, the dominant contributions to spin relaxation come from phonons emitted along certain directions, similar to the classical Cherenkov effect. Our calculation predicts a small correction to the Cherenkov angle caused by the quantum confinement. In the transition from subsonic to supersonic regime, we observe a peak in spin relaxation rate, which we term as a spin relaxation boom in analogy to the classical sonic boom.

The rest of the paper is organized as follows. In Section II we present our theoretical model and the derived spin relaxation rate. In Section III we analyze the angular distribution of the emitted phonons, focusing on the Cherenkov effect of directional phonon emission and effects of quantum confinement. In Section IV we clarify the overall spin relaxation in the different regimes of QD motion, with particular focus on spin relaxation boom and motion-dependence of the spin relaxation rate. In Section V we discuss the implications of our results, and in Section VI we present our conclusions. In addition, in the Appendices we give brief summaries of our theoretical derivations with regard to spin-orbit interaction in the context of a moving spin qubit.

II. MODEL AND SOLUTION

The system we consider is a single electron confined in a moving QD formed from a two-dimensional electron gas (2DEG), as is shown in Fig. 1. The qubit (electron) is moved at a constant speed v_0 , presumably achieved by programming the gates or using the surface acoustic waves. Conceptually, to ensure such a uniform linear motion for the electron, there has to be an external driving force, which we treat as a classical force. The total Hamiltonian [17, 22, 24] is given by

$$H = H_d + H_Z + H_{SO} + U_{ph}(r). \quad (2)$$

Here $H_d = \frac{\pi^2}{2m^*} + U[r - r_0(t)]$ is the orbital Hamiltonian for the moving QD, where $\pi = -i\hbar\nabla + (e/c)A(r)$ is the 2D momentum operator of the electron, and m^* is the effective mass of the electron. The motion we considered is linear: $r_0(t) = v_0 t$, and the QD confinement potential $U(r - r_0) = \frac{1}{2}m^*\omega_d^2(r - r_0)^2$ is quadratic. $H_Z = \frac{1}{2}g\mu_B B_0 \cdot \sigma$ is the Zeeman Hamiltonian, with B_0 the applied magnetic field. $H_{SO} = \beta_- \pi_y \sigma_x + \beta_+ \pi_x \sigma_y$ is the spin-orbit (SO) interaction, where $\beta_{\pm} = \beta \pm \alpha$ give the SO coupling strength, with α and β being the strengths of

Rashba [26] and Dresselhaus [27] SO interaction, respectively. Lastly, the electron-phonon interaction is given by [22, 24, 28]

$$U_{ph}(r) = \sum_{qj} \frac{F(q_z) e^{iq_{\parallel} \cdot r}}{\sqrt{2\rho_c \omega_{qj}/\hbar}} (e\beta_{qj} - iq\Xi_{qj}) (b_{-qj}^{\dagger} + b_{qj}), \quad (3)$$

where b_{qj}^{\dagger} and b_{qj} are the creation and annihilation operators for an acoustic phonon with wave vector $q = (q_{\parallel}, q_z)$ and branch index j , and ρ_c is the density of the material. The function $F(q_z) = \exp\left(-\frac{q_z^2}{2d^2}\right)$ models the confinement along z direction, where d is the characteristic width of the quantum well. We take into account both piezoelectric potential (β_{qj}) and deformation potential (Ξ_{qj}) in the electron-phonon interaction [28, 29]. By performing a Schrieffer-Wolff transformation to remove the SO coupling term to the first order [17, 22–24, 30], which we briefly summarize in Appendix A, the effective spin Hamiltonian can be obtained

$$H_{eff} = \frac{1}{2}g\mu_B[B_0 + \Delta B + \delta B(t)] \cdot \sigma, \quad (4)$$

where $\Delta B = \frac{2m^*}{g\mu_B}(\beta_- v_{0y}, \beta_+ v_{0x}, 0)$ is a motion induced constant magnetic field for the spin, and $\delta B(t) = 2B_0 \times \Omega(t)$ is the motion induced magnetic noise, where the time-dependent function $\Omega(t)$ originates from the phonon environment

$$\Omega(t) = \left\langle \psi \left| \frac{-1}{\hbar\omega_d^2} \left[\beta_- \frac{\partial U_{ph}}{\partial y}, \beta_+ \frac{\partial U_{ph}}{\partial x}, 0 \right] \right| \psi \right\rangle. \quad (5)$$

Here $|\psi\rangle$ is the instantaneous orbital ground state of the QD, so that $\langle \psi | \exp(iq \cdot r) | \psi \rangle = \exp[iq \cdot r_0(t)] e^{-q^2 \lambda^2/4}$, where $\lambda^{-2} = \hbar^{-1} \sqrt{(m^*\omega_d^2)^2 + (eB_z/2c)^2}$ is the total confinement length of the QD.

With the effective Hamiltonian (4), the spin relaxation rate can be obtained as (the detailed derivation is summarized in Appendix B)

$$\frac{1}{T_1} = \int_0^{\pi} d\theta \int_0^{2\pi} d\phi f(\theta, \phi), \quad (6)$$

where

$$f = \sum_j \frac{\hbar\omega_z F_{SO}}{(m^*\omega_d^2)^2} \frac{(2N_{w_z} + 1)}{8\pi^2 \rho_c v_j^4} w_z^4 \sin^3 \theta \cos^2 \phi C_{ep} F_z F_{xy}, \quad (7)$$

where

$$F_z = \exp\left(-\frac{d^2 w_z^2}{v_j^2} \cos^2 \theta\right), \quad F_{xy} = \exp\left(-\frac{\lambda^2 w_z^2}{2v_j^2} \sin^2 \theta\right), \quad (8)$$

are the cutoff functions in z direction and xy plane, respectively. They reflect the quantum confinement effect that will be discussed in the next section. The constant $C_{ep} = \left(e^2 \beta_{qj}^2 + \frac{w_z^2}{v_j^2} \Xi_{qj}^2\right)$ gives the total strength

of the two types of electron-phonon interaction, namely the deformation potential and the piezoelectric potential. $N_{w_z} = (e^{\hbar w_z/T} - 1)^{-1}$ is the number of phonons with frequency w_z at thermal equilibrium. The factor F_{SO} in Eq. (7) describes the angular dependence of the magnetic noise on the direction of the applied field, which can be expressed as $F_{SO} = (\beta^2 + \alpha^2)(1 + \cos^2 \theta_B) + 2\alpha\beta \sin^2 \theta_B \cos(2\varphi_B)$. Lastly, the angular dependence of kernel function f , and therefore the spin relaxation rate $1/T_1$, depends on a direction-dependent “shifted frequency” for the phonons,

$$w_z = \left| \frac{\omega_z}{1 - \xi_j} \right|, \quad (9)$$

instead of the spin Zeeman splitting $\omega_z = g\mu_B B_0/\hbar$. Here $\xi_j = \frac{v_0}{v_j} \sin \theta \cos(\phi - \phi_v)$. This is the Doppler shift in the context of moving spin relaxation.

In this model, spin relaxation is caused by the interaction between the electron and phonons from all directions. The double integration over θ and ϕ in Eq. (6) originates from the summation \sum_{qj} over all the phonon wave vectors q in Eq. (3). Therefore, the kernel function $f(w_z, \theta, \phi)$ describes contributions by phonons emitted or absorbed in the infinitesimal solid angle $d\theta d\phi$ around (θ, ϕ) . In our numerical calculations, we use typical parameters in a GaAs QD. There is one branch of longitudinal acoustic (LA) phonons, and two branches of transverse acoustic (TA) phonons. $v_1 = 4730$ m/s is the sound speed of the LA phonons, while $v_2 = v_3 = 3350$ m/s are the sound speed of the TA phonons. The strength of the deformation potential is $\Xi_1 = 6.7$ eV. The strengths of the piezoelectric interaction are $\beta_1(\theta) = 3\sqrt{2}\pi h_{14}\kappa^{-1} \sin^2 \theta \cos \theta$, $\beta_2(\theta) = \sqrt{2}\pi h_{14}\kappa^{-1} \sin 2\theta$, and $\beta_3(\theta) = \sqrt{2}\pi h_{14}\kappa^{-1} (3\cos^2 \theta - 1)$, where $h_{14} = -0.16$ C/m² and $\kappa = 13.1$ [22].

With the help of the analytical expression of the relaxation rate, in the next two Sections we examine in detail the features of the angular dependence of the kernel function f and the total relaxation rate $1/T_1$ for the moving spin qubit.

III. DIRECTIONAL PHONON EMISSION: DOPPLER EFFECT AND CHERENKOV RADIATION

In this Section we analyze the angular dependence of the phonon emission (in terms of the kernel function f) from the relaxing spin qubit in different regimes of QD moving speed. In particular, in the subsonic regime, we find the Doppler effect, in which phonons emitted in different directions have different frequencies. In the transonic regime we find the formation of a shock wave front and its bifurcation into two directions as the QD speed passes the speed of sound. Lastly in the supersonic regime we find a phonon analog of Cherenkov radiation, and identify a quantum confinement induced correction in the Cherenkov angle.

A. Doppler effect

When a QD moves relative to the lattice with a speed smaller than the speed of sound, the frequency of the phonon emitted or absorbed is shifted with a Doppler factor $\frac{1}{1 - \xi_j}$, as indicated in Eq. (9). In particular, in the forward direction ($\phi - \phi_v = 0$ and $\theta = \pi/2$), an emitted phonon has an increased frequency $\omega_z/(1 - v_0/v_j)$, while in the backward direction the phonon frequency is reduced to $\omega_z/(1 + v_0/v_j)$. These shifts are exactly as one would find in the classical Doppler effect.

It may seem puzzling that the energy quantum carried by the emitted phonon is not the same as the Zeeman splitting of the spin qubit. The discrepancy here can be accounted for by the fact that the moving quantum dot is an open system. It is driven by a classical force that comes from either programmed gate potential or the large number of phonons in an SAW. The excess or shortage of energy in the spin relaxation is absorbed/added by the classical “reservoir”.

B. Breaking the sound barrier

If the moving spin qubit acts classically, the transition from subsonic regime to supersonic regime (the transonic regime) for the moving spin qubit would be well represented by Fig. 1 (b), (c), and (d). At low speeds, presented in panel (b), there is no strongly directional emission. As the QD moving velocity becomes equal to the sound velocity, as indicated in panel (c), a single forward-propagating shock wave front is formed. When the moving velocity is larger than the critical velocity (d), the single shock wave front splits into two (We only consider the $x - y$ plane. In 3D the wave front is conical).

Quantum mechanically, we find that the moving spin qubit indeed follows qualitatively the classical behavior. Figure 2 shows the QD speed v_0 and angle ϕ dependence of the kernel function f (we have chosen $\theta = \pi/2$ to maximize f). When $v_0 < v_1$ [31], the angular distribution is relatively flat. When taking into account that phonon emission in spin relaxation is enabled by spin-orbit interaction, there is a pretty strong $\sin^3 \theta \cos^2 \phi$ angular dependence for f , so that emission along directions perpendicular to the direction of motion is suppressed. However, emissions along all other directions are allowed. When $v_0 \approx v_1$, the angular distribution in the xy plane rapidly becomes concentrated around $\phi = 0^\circ$, as $\phi = 0^\circ$ is a singularity of w_z when $v_0 = v_1$. Finally, when $v_0 > v_1$, the angular distribution in the xy plane is split into two branches. Each branch corresponds to an angle ϕ that gives the peak value of the kernel function f . As the moving velocity gradually increases from the subsonic regime to the supersonic regime, the kernel function gradually concentrates into the two bifurcating angles.

The transitions through the transonic regime can be more quantitatively seen from the cross sections given in Fig. 2 (b). For $v_0 = 2000$ m/s, which is subsonic, the

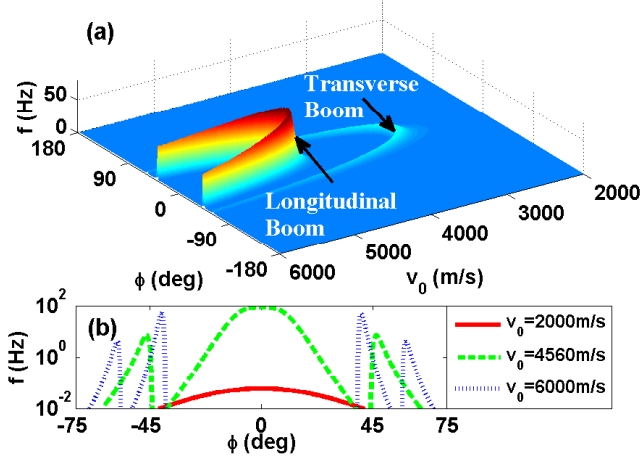


Figure 2. (color online) (a) Angular distribution (azimuthal angle ϕ) of the kernel function $f(\theta = \frac{\pi}{2}, \phi)$ for different moving velocity v_0 . Here the polar angle θ is fixed at $\theta = \frac{\pi}{2}$. The parameters are $B_0 = 1$ T, $\omega_d = 10.1$ meV, $d = 20$ nm, $\phi_v = 0$. (b) Three cross-sections of (a) at different velocities. The red solid line has a velocity below the speed of the transverse acoustic phonons; the green dashed line has a velocity at the speed of longitudinal acoustic phonons, and the blue dotted line has a velocity above the speed of longitudinal phonons.

kernel function is smooth and has a small magnitude. At $v_0 = 4560$ m/s, the speed of sound for the LA phonons, a large peak appears at $\phi = 0$. Notice that the logarithmic scale has made this peak appears to be broader than it really is (the logarithmic scale is necessary for us to see the subsonic value of f). The two side peaks are the shock waves produced by the TA phonons, for whom the moving dot is already supersonic. Lastly, at $v_0 = 6000$ m/s, the moving qubit is supersonic with respect to both LA and TA phonons. Thus two sets of shock wave peaks appear for the kernel function in this case.

C. The Cherenkov effect

We now examine the supersonic regime more closely, where we find clear evidence of Cherenkov radiation of phonons from the moving spin qubit. In Fig. 3, we plot the kernel function f as a function of azimuthal angle θ and polar angle ϕ when the QD speed is $v_0 = 6000$ m/s, larger than the speed of sound for both LA (v_1) and TA (v_2) phonons. Clearly, **the dominant contribution to spin relaxation is concentrated in two particular directions in the xy plane** (at $\phi \approx \pm 40^\circ$ and $\theta \approx 90^\circ$). These peaks come from deformation potential interaction with LA phonons. Two much smaller peaks appear near $\phi \approx 60^\circ$ and $\theta \approx 90^\circ$, which originates from piezoelectric interaction with TA phonons.

Strong angular concentration is a typical characteristic of the Cherenkov effect. In the current case, the emitted/absorbed phonons have a Doppler shifted frequency

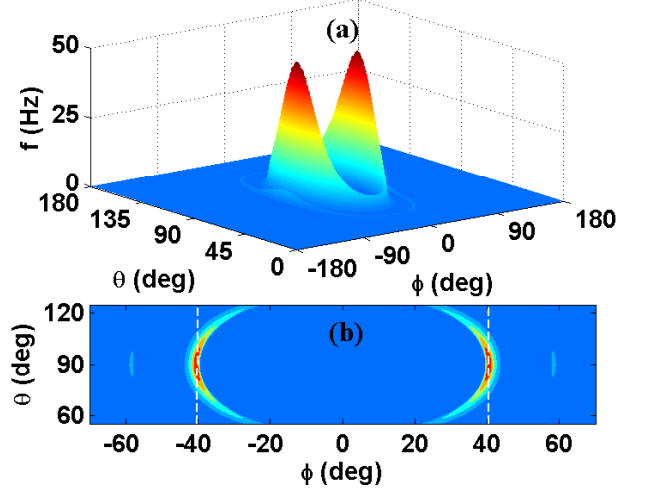


Figure 3. (color online) (a) Angular distribution of the kernel function $f(\theta, \phi)$. (b) Contour plot of $f(\theta, \phi)$ in a small region. The parameters are chosen as $v_0 = 6000$ m/s, $B_0 = 1$ T, $\omega_d = 0.01$ eV, $d = 20$ nm, $\phi_v = 0$.

of $w_z = \omega_Z / (1 - \xi_j)$. Without considering the quantum confinement effect embodied by the cutoff functions F_z and F_{xy} , the kernel function f in Eq. (7) is proportional to w_z^4 (we limit our consideration here to the deformation potential interaction with LA phonons. The discussion is similar when piezoelectric interaction dominates), and diverges when $\xi_j = 1$. Thus the angular distribution should peak along the directions given by $\xi_j = 1$, i.e.,

$$\sin \theta \cos(\phi - \phi_v) = \frac{v_j}{v_0}, \quad (10)$$

which is identical to the classical Cherenkov relation in Eq. (1). For the parameters used to generate Fig. 3, Eq. (10) gives a Cherenkov angle of $\phi_C \approx 38^\circ$ at $\theta = \pi/2$, only slightly smaller (although qualitatively significant, as we discuss in the next subsection) than the numerical value give in the figure.

In addition to the small discrepancy in the Cherenkov radiation angle, a more significant difference between Eq. (10) and Fig. 3 is that the equation predicts a conical wave front for the shock wave, while the numerical results present in the figure have a strong two-dimensional characteristic. The bend in the peaks in Fig. 3 can be explained by the $\sin \theta$ factor in Eq. (10), but the suppression of the peaks away from $\theta = \pi/2$ cannot. We need to include all the factors in Eq. (7) to explain this difference, as we will do in the next subsection.

D. Quantum correction on Cherenkov angle

While Eq. (10) is consistent with the classical result, our situation of the moving spin qubit is more nuanced. Indeed, $\xi_j = 1$ would lead to a diverging phonon frequency w_z , which is clearly unphysical. A more accurate

description of the phonon Cherenkov radiation from a moving spin qubit can only be obtained when quantum confinement effects are taken into account.

Mathematically, quantum confinement effects are incorporated in the cutoff functions F_z and F_{xy} in Eq. (8), which are exponentially decaying functions of the phonon frequency w_z . Since F_z and F_{xy} decay much faster than the increase in the power function w_z^4 , the singularity of $w_z \rightarrow \infty$ is eliminated, and the peak value of the kernel function f is shifted from infinity to a large yet finite number. Physically, the cutoff functions are simply a reflection of the phonon bottleneck effect [32, 33]: for an electron with a finite width λ in its wave function, the interaction matrix element $\langle e^{iq_{\parallel} \cdot r} \rangle$ is suppressed if the phonon wave length is much smaller than λ .

For a gated QD in semiconductor nanostructures (such as a gated depletion dot from a two-dimensional electron gas), the confinement in z direction (growth direction) is much stronger than those in the xy directions (in-plane directions), so that phonons are only emitted in the xy plane. This explains the more two-dimensional nature of f in Fig. 3, instead of a conical shape. When confined to the xy plane, the kernel function f is reduced to

$$f = \sum_j \frac{\hbar\omega_Z F_{SO}}{(m^*\omega_d^2)^2} \frac{(2N_{w_z} + 1)}{8\pi^2 \rho_c v_j^5} w_z^4 \cos^2 \phi F_{xy} C_{ep}, \quad (11)$$

with $\xi_j = \frac{v_0}{v_j} \cos \phi$ (assume $\phi_v = 0$). Now the kernel function f depends on the phonon frequency w_z as $f \propto w_z^4 \exp(-w_z^2 \lambda^2 / 2v_1^2)$ (instead of $f \propto w_z^4$ when confinement effect is not included). The peak of f thus appears at

$$w_z = \frac{2v_1}{\lambda}. \quad (12)$$

Using the parameters in Fig. 3, the peak value of f occurs at $w_z = 8.9 \times 10^{11} \text{ s}^{-1}$, while the Zeeman frequency is $3.87 \times 10^{10} \text{ s}^{-1}$ (at $B = 1 \text{ T}$). With $w_z/\omega_Z \approx 23$, the phonon energy has been Doppler-shifted greatly, from about $25 \text{ } \mu\text{eV}$ for $\hbar\omega_Z$ to nearly $600 \text{ } \mu\text{eV}$ for $\hbar w_z$. Recall that $w_z = \frac{\omega_Z}{1 - v_0 \cos \phi / v_1}$, Using Eq. (12) it is straight forward to obtain

$$\phi'_C = \arccos\left(\frac{v_1}{v_0} - \frac{\omega_Z \lambda}{2v_0}\right). \quad (13)$$

Clearly, quantum confinement for the spin qubit leads to the correction term $-\frac{\omega_Z \lambda}{2v_0}$. Using the parameters in Fig. 3, with an applied field of 1 T and QD speed of $v_0 = 6000 \text{ m/s}$ (with the speed of sound for LA phonons at $v_1 = 4730 \text{ m/s}$ in GaAs), we obtain

$$\phi \approx \pm 40^\circ. \quad (14)$$

This is consistent with the results shown in Fig. 3, where the peak in the kernel function f appears at $\phi \approx \pm 40^\circ$ for $\theta = \pi/2$.

In short, a combination of the Cherenkov effect and quantum confinement leads to the results presented in

Fig. 3. The quantum confinement for the QD that carries the spin qubit makes the phonon emission more two-dimensional. It also suppresses the electron interaction with higher-energy phonons, leading to a small correction to the Cherenkov radiation angle and a significant modification to the energy of the radiated phonons. Another consequence of the quantum confinement is that the velocity when “spin-relaxation boom” occurs is also slightly shifted, as we discuss in the next Section.

IV. SPIN RELAXATION IN A MOVING QUANTUM DOT

In the last Section we have examined in detail the angular behavior of phonon emission in the relaxation of a moving spin qubit. In this Section we focus on the integrated effect of QD motion on spin relaxation. We are particularly interested in how spin relaxation varies with the speed of the QD motion and the applied magnetic field.

Classically, the drag force on an aircraft increases sharply when the aircraft velocity approaches the sound barrier. This is the so-called sonic boom. We find a similar behavior in the relaxation rate for a moving spin qubit. In Fig. 4, we plot the spin relaxation rate $1/T_1$ as a function of the QD speed v_0 . The curve of the total relaxation rate (black, dot-dashed) peaks at the two sound barriers due to TA (at $v_2 = v_3$) and LA phonons (at v_1). Each peak for a single type of phonons (for example, the red curve for the LA phonons) is similar to the Prandtl-Glauert singularity [34] for the classical “sonic boom”. These peaks can thus be named “spin-relaxation boom”. The total relaxation is a simple sum of contributions from LA and TA phonons. The quantum confinement again produces some modifications to these booms. First, the singularities are eliminated and broadened into smooth and finite peaks. Second, the peaks are shifted downward from v_1 and v_2 .

One implication of the spin relaxation booms presented above is that a spin qubit can relax slower when the QD moves faster, as evidenced by the curves in Fig. 4. In Fig. 5 (a) we give a more comprehensive plot of this velocity dependence. Here we plot the spin relaxation rate as a function of the moving velocity v_0 and the magnetic field B_0 . When the external magnetic field is weak (e.g., $B_0 \approx 2 \text{ T}$), the relaxation rate increases with the moving velocity. But when the external magnetic field is strong (e.g., $B_0 > 5 \text{ T}$), the relaxation rate becomes a decreasing function of the moving velocity. This somewhat counterintuitive feature can be understood with the help of the “shifted frequency” w_z for the emitted phonon, which depends on both the magnetic field B_0 and the moving velocity v_0 . When the moving velocity is fast, the Doppler effect is strong, leading to the “shifted frequency” to get into the range where phonon bottleneck effect suppresses electron-phonon interaction, as we have

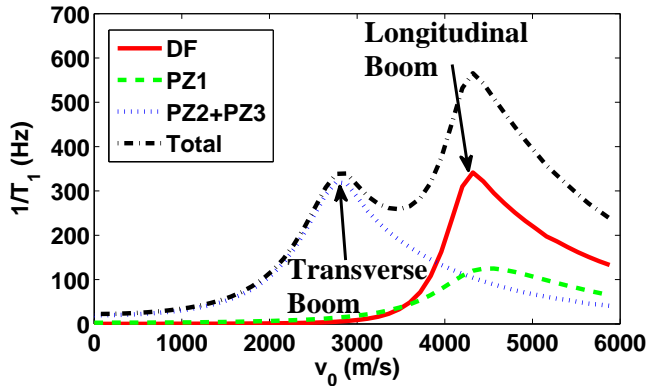


Figure 4. (color online) Spin relaxation rate $1/T_1$ as a function of moving velocity v_0 . The red (solid), green (dashed), blue (dotted), and black (dot-dashed) lines represent the deformation, the longitudinal piezoelectric, the transverse piezoelectric and the total spin relaxation rate respectively. The parameters are chosen as $B_0 = 2$ T, $\omega_d = 3.1$ meV, $d = 20$ nm, $\phi_v = 0$.

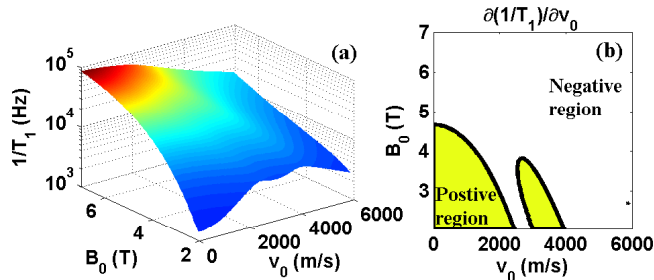


Figure 5. (color online) (a) Spin relaxation rate $1/T_1$ as a function of magnetic field B and moving speed of the quantum dot v_0 . (b) Partial derivative of $1/T_1$ with respect to v_0 . The white and the yellow regions indicate the partial derivative is below and above zero respectively. The parameters are chosen as $\omega_d = 1.1$ meV, $d = 20$ nm, $\phi_v = 0$.

discussed in subsection III D. The “shifted frequency” w_z also depends on the magnetic field B_0 . In a strong field, the Zeeman frequency ω_Z is already close to the bottleneck regime. It is thus much easier for Doppler effect to shift the frequency higher and suppress the phonon coupling.

Our observation here indicates that a moving spin qubit may have an even lower relaxation rate than a static spin qubit. While “motional narrowing” is a common occurrence in spin resonance experiments [35], suppressing decoherence by moving a spin qubit faster in a nanostructure setting is still an intriguing proposition. In Fig. 5 (b), we plot the partial derivative of $1/T_1$ with respect to v_0 . Here the white region indicates where spin relaxation can be suppressed by increasing the moving velocity, since in this region the partial derivative of $1/T_1$ with respect to v_0 is negative. On the other hand, in the yellow region the partial derivative with respect to v_0 is positive,

and relaxation becomes faster when the spin qubit moves faster. In short, the motional narrowing effect here shows the possibility of coherence-preserving transportation of a spin qubit.

V. DISCUSSIONS

Our study shows that in the supersonic regime for a moving spin qubit, only phonons emitted or absorbed in certain directions make notable contributions to qubit relaxation. As is shown in Fig. 3, the kernel function f for the spin relaxation rate $1/T_1$ is non-zero only in certain directions in the xy plane. With this strong angular anisotropy, it is natural to consider whether we could eliminate spin relaxation by suppressing the electron-phonon interaction in certain directions. For example, if a phonon cavity is set up in a certain direction, the frequencies of phonon modes in that direction become discrete, making it possible to filter out important frequencies and to suppress electron-phonon interaction at those frequencies.

The narrowly directional phonon emission from the moving spin qubit may also be used as a source of phonons. Imagine an SAW provides a stream of excited spins and they also emit phonons in one direction. If a phonon cavity is set up along that direction and is on resonance with the emitted phonons, it may be possible to create stimulated emission, even lasing, of phonons in that mode [36].

The interesting features in phonon emission and spin relaxation we have explored here could be useful in monitoring and detecting the spin decoherence process. Conversely, knowing the phonon emission angle precisely may allow continuous monitoring of the environment, which could in turn provide more accurate information to possible feedback operations in a quantum feedback control [37, 38] or quantum state restoration [39, 40] scheme. In an open quantum system, the information stored in the system constantly leaks into its environment. By measuring the environment in particular ways, however, the lost information could be fully or partially regained. It is thus possible to restore a system to its initial state by performing certain operations [40]. Our results about the angular distribution of phonon emission may provide a guidance on measuring the phonon environment: we can place the phonon detectors in selected directions [precisely predicted by Eq. (13)] since only phonons in those directions make significant contributions to spin relaxation.

VI. CONCLUSIONS

In this work we have studied decoherence of a moving spin qubit caused by phonon noise through spin-orbit interaction. We find that the QD motion leads to Doppler shifts in the emitted/absorbed phonons by the moving

spin qubit. When the moving velocity is larger than the sound velocity in the material, spin relaxation is dominated by phonon emission/absorption in certain directions. The physics here is similar to the phenomenon of classical Cherenkov radiation. We derive an explicit formula for the quantum confinement correction to the Cherenkov angle. We also find a “spin-relaxation boom” when the moving QD break the sound barriers, in analogy to the classical sonic boom. The spin relaxation rate peaks when the QD velocity matches the speed of sound for a particular phonon branch. It is possible to reduce decoherence by increasing the moving velocity. Indeed, in the supersonic regime, the moving spin qubit may have an even lower decoherence rate than a static qubit.

Our study on the relaxation of a moving spin qubit sheds new light on the topic of spin-phonon interaction in a semiconductor nanostructure. There could be significant implications in a wide range of subject areas, from quantum coherent operations such as transferring and preserving quantum information to more classical applications such as coherent phonon optics.

ACKNOWLEDGMENTS

We thank fruitful discussions with Jo-Tzu Hung, and acknowledge financial support by US ARO (W911NF0910393) and NSF PIF (PHY-1104672).

Appendix A: Derivation of the effective Hamiltonian

An effective spin Hamiltonian, in which spin dynamics and orbital dynamics are decoupled, can be obtained by performing a Schrieffer-Wolff transformation to remove the SO coupling term in the full Hamiltonian [17, 22–24, 30]. Through a unitary transformation $\tilde{H} = e^S H e^{-S}$, with S given by $[H_d + H_Z, S] = H_{SO}$, the SO coupling is removed to the first order. The spin Hamiltonian is then $H_{eff} = \langle \psi | \tilde{H} | \psi \rangle$, where $|\psi\rangle$ is the ground state of the orbital wave function. Following the approach used in Refs. [17, 22], we obtain the effective Hamiltonian in Eq. (4), where $\Omega(r, t)$ originates from the electron-phonon interaction, and is given explicitly as

$$\Omega_x(t) = \sum_{qj} -\frac{\beta_-}{\hbar\omega_d^2} \frac{iq_y F(q_z) e^{-q^2\lambda^2/4}}{\sqrt{2\rho_c\omega_{qj}/\hbar}} \times (e\beta_{qj} - iq\Xi_{qj}) e^{iq\cdot r_0(t)} (b_{-qj}^\dagger + b_{qj}), \quad (\text{A1})$$

$$\Omega_y(t) = \sum_{qj} -\frac{\beta_+}{\hbar\omega_d^2} \frac{iq_x F(q_z) e^{-q^2\lambda^2/4}}{\sqrt{2\rho_c\omega_{qj}/\hbar}} \times (e\beta_{qj} - iq\Xi_{qj}) e^{iq\cdot r_0(t)} (b_{-qj}^\dagger + b_{qj}). \quad (\text{A2})$$

The expressions here are similar to the results in Ref. [22], with an additional term $e^{iq\cdot r_0(t)}$ due to the motion of the quantum dot. This factor is also how Doppler effect is introduced into the dynamics of the moving spin qubit.

Appendix B: Derivation of the spin relaxation rate

Given the effective Hamiltonian (4), the relaxation rate can be obtained within the Bloch-Redfield theory as $\frac{1}{T_1} = J_{XX}^+(\omega_Z) + J_{YY}^+(\omega_Z)$ [24], where $\omega_Z = g\mu_B/\hbar$ is the Zeeman frequency. The tensors J_{XX}^+ and J_{YY}^+ are correlations of the effective magnetic noise (from the phonons through the SO interaction),

$$J_{ij}^+(\omega) = \frac{g^2\mu_B^2}{4\hbar^2} \text{Re} \int_{-\infty}^{\infty} \langle \{\delta B_i(0), \delta B_j(t)\} \rangle e^{-i\omega t} dt. \quad (\text{B1})$$

These correlation functions are expressed in a rotated XYZ coordinate system, where the Z axis is along the direction of the applied field B_0 . Due to this rotation, a magnetic-angular dependence term F_{SO} appears in the expression of the relaxation rate [22, 24]. With the magnetic noise from phonons, the relaxation rate takes the form

$$\frac{1}{T_1} = F_{SO}\omega_Z^2 \text{Re} \int_{-\infty}^{\infty} dt \sum_j \int d\theta \int d\phi \int d\omega_j e^{-i\omega_Z t} \frac{\omega_j^3}{v_j^5} \times \frac{\sin^3 \theta \cos^2 \phi}{(\hbar\omega_d^2)^2} \frac{|F(\frac{\omega_j}{v_j} \cos \theta)|^2 e^{-q^2\lambda^2/2}}{(2\pi)^3 2\rho_c/\hbar} C_{ep} A, \quad (\text{B2})$$

where

$$A \equiv \left\langle b_{qj}^\dagger b_{qj} e^{-i\omega_{qj}(1-\xi_j)t} + b_{qj} b_{qj}^\dagger e^{i\omega_{qj}(1-\xi_j)t} \right\rangle + \left\langle b_{qj}^\dagger b_{qj} e^{i\omega_{qj}(1-\xi_j)t} + b_{qj} b_{qj}^\dagger e^{-i\omega_{qj}(1-\xi_j)t} \right\rangle. \quad (\text{B3})$$

Compared with Ref. [22], the phonon frequency here is shifted by the factor $(1 - \xi_j)$, which is a result of the Doppler effect. After performing the time integral in Eq. (B2) we obtain the relaxation rate (6) and the kernel function (7). When the moving velocity approaches zero, the relaxation rate here reduces exactly to the result shown in Ref. [17].

- [2] G. Balasubramanian *et al.*, Nat. Mater. **8**, 383 (2009).
- [3] H. Bluhm, S. Foletti, I. Neder, M. Rudner, D. Mahalu, V. Umansky, and A. Yacoby, Nat. Physics **7**, 109 (2011).
- [4] J. T. Muhonen *et al.*, Nat. Nanotechnol. **9**, 986 (2014).
- [5] R. Hanson, L. P. Kouwenhoven, J. R. Petta, S. Tarucha, and L. M. K. Vandersypen, Rev. Mod. Phys. **79**, 1217 (2007).
- [6] J. J. L. Morton, D. R. McCamey, M. A. Eriksson, and S. A. Lyon, Nature **479**, 345 (2011).
- [7] D. D. Awschalom, L. C. Bassett, A. S. Dzurak, E. L. Hu, J. R. Petta, Science **339**, 1174 (2013).
- [8] C. H. W. Barnes, J. M. Shilton, and A. M. Robinson, Phys. Rev. B **62**, 8410 (2000).
- [9] A. J. Skinner, M. E. Davenport, and B. E. Kane, Phys. Rev. Lett. **90**, 087901 (2003).
- [10] A. D. Greentree, J. H. Cole, A. R. Hamilton, and L. C. L. Hollenberg, Phys. Rev. B **70**, 235317 (2004).
- [11] J. M. Taylor, H. A. Engel, W. Dür, A. Yacoby, C. M. Marcus, P. Zoller, and M. D. Lukin, Nat. Phys. **1**, 177 (2005).
- [12] J. A. H. Stotz, R. Hey, P. V. Santos, and K. H. Ploog, Nat. Mater. **4**, 585 (2005).
- [13] S. Hermelin, S. Takada, M. Yamamoto, S. Tarucha, A. D. Wieck, L. Saminadayar, C. Bauerle, and T. Meunier, Nature (London) **477**, 435 (2011).
- [14] R. P. G. McNeil, M. Kataoka, C. J. B. Ford, C. H. W. Barnes, D. Anderson, G. A. C. Jones, I. Farrer, and D. A. Ritchie, Nature (London) **477**, 439 (2011).
- [15] H. Sanada, T. Sogawa, H. Gotoh, K. Onomitsu, M. Kohda, J. Nitta, and P. V. Santos, Phys. Rev. Lett. **106**, 216602 (2011).
- [16] M. Yamamoto, S. Takada, C. Bauerle, K. Watanabe, A. D. Wieck, and S. Tarucha, Nat. Nanotech. **7**, 247 (2012).
- [17] P. Huang and X. Hu, Phys. Rev. B **88**, 075301 (2013).
- [18] M. V. Nezlin, Sov. Phys. Usp. **19**, 946 (1976).
- [19] V. L. Ginzburg 1996 Phys. Usp. **39**, 973 (1996).
- [20] J. V. Jelley, J. Appl. Phys. **6**, 227 (1955).
- [21] S. Smirnov, Phys. Rev. B **83**, 081308(R) (2011).
- [22] V. N. Golovach, A. Khaetskii, and D. Loss, Phys. Rev. Lett. **93**, 016601 (2004).
- [23] M. Borhani, V. N. Golovach, and D. Loss, Phys. Rev. B **73**, 155311 (2006).
- [24] V. N. Golovach, M. Borhani, and D. Loss, Phys. Rev. B **74**, 165319 (2006).
- [25] V. K. Dugaev, E. Y. Sherman, V. I. Ivanov, and J. Barnas, Phys. Rev. B **80**, 081301 (2009).
- [26] Y. A. Bychkov and E. I. Rashba, J. Phys. C **17**, 6039 (1984).
- [27] G. Dresselhaus, Phys. Rev. **100**, 580 (1955).
- [28] G. D. Mahan, *Many-Particle Physics* (Plenum, New York, 1981).
- [29] V. F. Gantmakher and Y. B. Levinson, *Carrier Scattering in Metals and Semiconductors* (North-Holland, Amsterdam, 1987).
- [30] P. Huang and X. Hu, Phys. Rev. B **89**, 195302 (2014).
- [31] For the parameters used in this paper, deformation potential coupling to LA phonons provides the dominant spin relaxation channel. Therefore the critical velocity for Cherenkov effect is approximately v_1 . For a case when piezoelectric potential is dominant or when both interactions are important, there would be two critical velocities, determined by the two types of phonons.
- [32] J. Urayama, T. B. Norris, J. Singh, and P. Bhattacharya, Phys. Rev. Lett. **86**, 4930 (2001).
- [33] P. Huang and X. Hu, Phys. Rev. B **90**, 235315 (2014).
- [34] A. H. Shapiro, *Compressible Fluid Flow I*, (Wiley, New York, 1953).
- [35] C.P. Slichter, *Principles of Magnetic Resonance* (Springer-Verlag, Berlin, 1980).
- [36] A. Khaetskii, V. N. Golovach, X. Hu, I. Žutić, Phys. Rev. Lett. **111**, 186601 (2013).
- [37] H. M. Wiseman and G. J. Milburn, Phys. Rev. Lett. **70**, 548 (1993).
- [38] H. M. Wiseman, Phys. Rev. A **49**, 2133 (1994);
- [39] X. Zhao, S. R. Hedemann, and T. Yu, Phys. Rev. A **88**, 022321 (2013).
- [40] K. Wang, X. Zhao, and T. Yu, Phys. Rev. A **89**, 042320 (2014).